Pyrolysis and Isomerization of Quadricyclane, Norbornadiene, and Toluene

Zhi Li and Scott L. Anderson*

Department of Chemistry, University of Utah, Salt Lake City, Utah 84112

Received: July 13, 1998

Pyrolysis and isomerization of the C_7H_8 isomers quadricyclane, norbornadiene, cycloheptatriene, and toluene have been studied in a micro-flow tube reactor with detection/isomer identification by guided-ion beam tandem mass spectrometry. The methodology permits pyrolysis studies with product isomer identification with samples of only a few milligrams. The samples are premixed with buffer gas and then passed through a temperature-controlled flow tube reactor with millisecond residence time. The sample/pyrolysis products exiting the flow tube are ionized by methane chemical ionization (CI), and both CI mass spectra and low-energy collision-induced dissociation were used to determine the composition. For the experimental residence time, toluene and cycloheptatriene are stable over the 298−998 K temperature range. Decomposition of norbornadiene sets in at ~600 K. The dominant decomposition processes are acetylene elimination via a retro-Diels−Alder reaction and isomerization to toluene. Quadricyclane begins to decompose at ~500 K, and the dominant decomposition processes are the acetylene elimination and isomerization to toluene, with a small amount of norbornadiene production. The results are discussed in relation to previous studies at lower temperatures/longer times.

I. Introduction

Strained hydrocarbons, such as cubane or quadricyclane, are an interesting class of molecules, both from a fundamental perspective and because they have potential as high-energy density materials. The high volumetric energy density arises mostly from the fact that these molecules tend to be denser than normal hydrocarbons; however, the built-in strain energy raises the possibility that combustion mechanisms might be significantly different as well. There is current interest[1−6] in trying to tailor the physical and chemical properties of these potential fuel molecules by derivatization. Since synthesis is nontrivial, new molecules are typically available only in milligram quantities, while standard methods for screening combustion/pyrolysis behavior require substantially larger samples. We have developed a method, described here, to analyze pyrolysis behavior with small samples. From our measurements we not only get thermal breakdown behavior but also can identify the decomposition products and learn something about the mechanism. The details of the soft ionization/low-energy ion dissociation method used for isomer identification have been reported recently.[7] This paper reports our initial pyrolysis study on quadricyclane (QC) and its isomers norbornadiene (NBD), cycloheptatriene (CHT), and toluene (TOL).

Quadricyclane and its isomers have been the subject of both experimental and theoretical investigation for about four decades, making it a good test system. On the other hand, all previous pyrolysis work has been at relatively low temperatures/long reaction times, far from conditions relevant to combustion chemistry. The thermochemistry for both the neutral and ionic systems is summarized in Figure 1. The heats of formation and barrier heights have been taken from Lias et al.,[8] Bach et al.,[9] Birely and Chesick,[10] and Lishan et al.[11]

Early experimental work on the C_7H_8 system includes studies of pyrolysis of NBD and cycloheptatriene (CHT), isomerization of CHT to TOL,[12−15] and interconversion between QC and NBD.[16,17] More recently, there have been reports of QC photochemistry,[11] quantum calculations of isomerization energetics,[9] and photodetachment[18] and flow tube studies[19] of $C_7H_7^-$ produced by deprotonation of QC and its isomers.[19] In this latter study, the gas-phase acidity order of these C_7H_8 isomers was determined along with the C−H bond dissociation energy of QC. Two good reviews of recent literature on C_7H_8 isomers are given by Kuck[20] and Gunion et al.[18]

In the previous pyrolysis studies it has been found that CHT can be converted to TOL by photoexcitation in the gas phase.[14] NBD is reported to rearrange to TOL via a CHT intermediate and to break down by a retro-Diels−Alder process to cyclopentadiene and acetylene upon heating to between 400 and 475 °C (see Woods et al.[12] and references therein). An important result is that NBD can be converted to QC by ultraviolet irradiation and converted back to NBD by heating to 400−500 K.[17,16] This reversible interconversion has been proposed as a method for direct storage of solar energy.[21−24] Kinetics and quantum calculations indicate that the activation energy (E_a) of the QC → NBD isomerization is ~141 kJ/mol (33.9 kcal/mol) and the E_a for the ionic $QC^{\bullet+} \rightarrow NBD^{\bullet+}$ isomerization is ~46 kJ/mol (11 kcal/mol) (see Bach[9] and references therein).

II. Experimental Section

The experiments are performed using a low-energy guided-ion beam tandem mass spectrometer coupled to a heatable micro-flow tube. The instrument and mass spectrometric techniques for analyzing the composition of the mixture exiting the flow tube have been described elsewhere.[7] Here we give only an overview of the instrument and methods, followed by a description of the important properties of the flow tube and data-fitting procedures.

Overview. The organic molecules of interest are premixed with an inert buffer gas (argon or helium) at ~5−7% concentration, in an inlet system entirely constructed of glass and Teflon. The nominal concentration is controlled by setting the pressure of buffer gas flowing past a sample vial containing the liquid

10.1021/jp9829905 CCC: $15.00 © 1998 American Chemical Society
Published on Web 10/27/1998

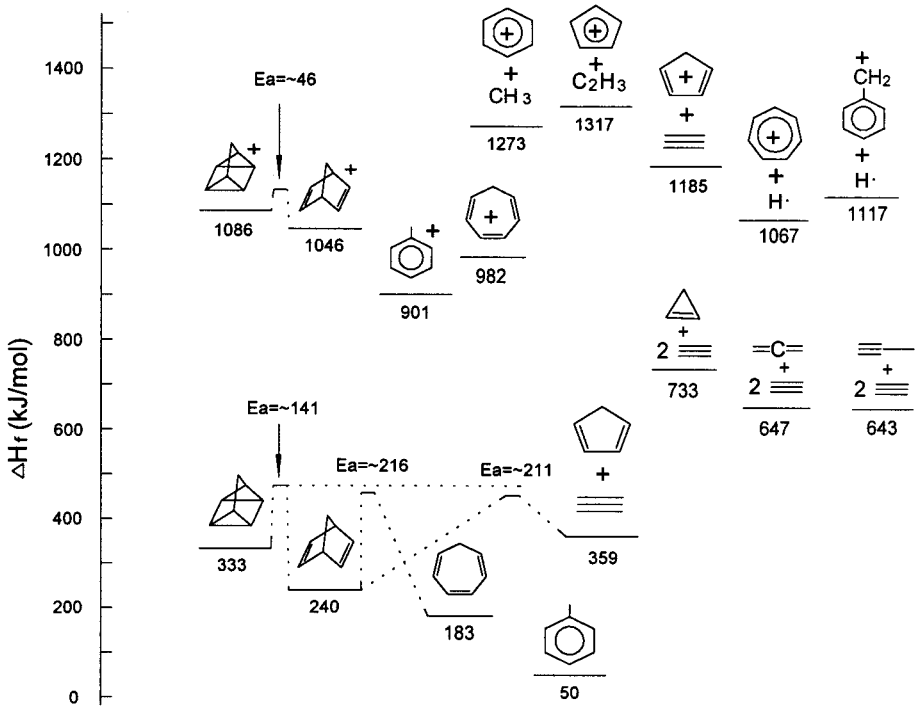

Figure 1. Energetics of the C_7H_8 and $C_7H_8^+$ systems.

sample material at room temperature. The flow velocity at this point in the inlet system is slow enough that diffusion is efficient at mixing the sample into the buffer. The actual concentration is checked by simply measuring sample consumption rate over the course of a set of experiments and is typically 80−90% of the nominal concentration. The sample-laden flow is then passed through a glass/Teflon leak valve at constant mass flow rate and into the micro-flow tube reactor. The flow tube is simply a 30 cm long quartz tube with 1.9 mm inside diameter. The final 10 cm of the tube is encased in a heater that can raise the temperature to 1000 K.

The flow tube empties directly into a high-pressure ion source. The coupling is done by inserting the final 3 mm of the tube into a counterbore in the source that is 0.1 mm larger than the o.d. of the tube. This creates an annular gap that reduces the thermal conductivity between the flow tube and source but still gives a low conductance ($\sim 2 \times 10^{-4}$ L/s) leak path out of the source. This source is essentially a sealed box with internal dimensions of 15.5 × 15.5 × 23 mm. In addition to the gas inlet from the flow tube, there is an inlet for the CI reagent gas, in this case CH_4. A 0.58 mm hole allows a magnetically collimated electron beam to be injected into the source volume, and a second 0.99 mm hole is located perpendicular to the e-beam to allow ions to escape. The ion source temperature is mainly determined by radiant and e-beam heating from the electron gun, but there is a small effect of heat transfer from the flow tube at higher flow tube temperatures. To avoid having ion source conditions dependent on the flow tube temperature, the ion source block is maintained at a constant temperature (350 K) by an auxiliary heater. Because the temperature and mass flow rate are both constant, the total ion source pressure is also constant at ~0.51 Torr. The source is designed such that the analyte gas flows around a repeller to mix with the CI reagent gas before passing into the ionization region. The analyte molecules are, thus, thermalized at the source temperature before ionization, and we expect no significant effects of flow tube temperature on ionization efficiency or ion cracking patterns.

The ions are injected into a radio-frequency (rf) octapole that guides them through a differential pumping wall and up to the first mass filter. This is a quadrupole that has been specially optimized to mass select without perturbing the kinetic energy distribution of the transmitted ions.[25] This mass filter can either be used to select a particular ion mass for further study or be operated in non-mass selective mode. The transmitted ions are injected into a two-section rf octapole that guides the beam through a scattering cell, where collisions with xenon can be used to fragment the ions selected by the first mass filter. The octapole collects product ions together with unreacted primary ions and guides them to the final quadrupole mass analyzer, after which they are counted by a Daly detector[26]/CAMAC scalar combination.

As will be seen below, the methane CI source creates a background of hydrocarbon cations, much weaker than the signal, but nonetheless causing some detection problems. We attempted to circumvent the hydrocarbon background problem by using several non-hydrocarbon CI reagents (OCS^+, Xe^+, NO^+). Unfortunately, OCS^+ and Xe^+ appear to create hot analyte ions and thus largely eliminate our ability to distinguish QC and NBD. NO^+ mostly gives $(M - 1)^+$ by hydride abstraction and again renders the isomers nearly indistinguishable.

Flow Tube. The flow tube reactor is a 1.9 mm diameter, low flow rate device, in keeping with our need to minimize sample consumption for the synthetic strained molecules of interest. As discussed below, this imposes some limitations on the interpretation of the data.

The pressure, flow characteristics, and residence time in the hot zone of the flow tube are estimated as follows. The flow rate of the argon/hydrocarbon mixture is controlled by a glass/Teflon metering valve upstream of the flow tube. The pressure drops from ~500 to ~15 Torr across the valve, and this large pressure difference ensures that the mass flow rate set by the valve is constant to within a few percent despite small changes in the downstream pressure with flow tube temperature. The pressure in the source vacuum chamber is monitored by an

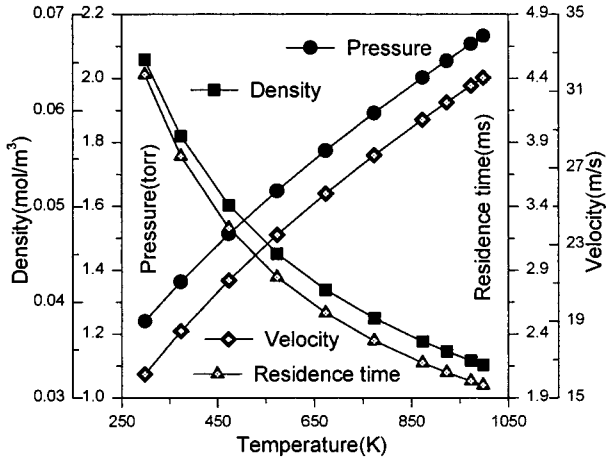

Figure 2. Temperature dependence of important flow tube properties.

ionization gauge and combined with the pumping speed (600 L/s for argon) and gauge sensitivity factor; this allows us to calculate the total flow rate. The flow rate was typically set to 0.057 Torr L/s (=0.0076 Pa·m^3/s), corresponding to a total mass flow rate of 0.16 kg·s^{-1} m^{-2}, or ~23 μg/s. Since only ~5−7% of the total flow is the strained-molecule sample, the nominal sample consumption rate is only around 1 μg/s, allowing hours of experimentation with the ~20 mg sample typically available to us. The actual consumption rate is measured by weight loss over the course of the experiments. For example, under our normal operating conditions, the actual consumption rate for toluene was ~0.9 μg/s.

From the conductance out of the ion source, we can calculate the ion source pressure, which is also the exhaust pressure of the flow tube. With no flow of methane CI reagent, the flow tube exit pressure is 0.33 Torr for pure argon flow. Because our hydrocarbon sample concentration is small, the conditions should be essentially identical for the sample-laden flow.

The Reynolds number of the flow ranges from ~3.5 to ~1.5 over the temperature range from 298 to 1000 K. This is well within the non-turbulent flow regime, and fully developed laminar flow is established well upstream of the hot zone of the flow tube. We can thus use the standard isothermal compressible flow equations,[27] with appropriate parameters for low Reynolds number flow, to calculate the pressure and flow velocity in the upstream and hot zone sections of the flow tube. Figure 2 gives the temperature dependence of the hot zone pressure, density, mass-flow-weighted velocity, and mass-flow-weighted residence time. The values plotted are for the midpoint of the hot zone (i.e., 5 cm upstream from the source). As shown, both the density and residence time decrease by about a factor of 2 over the temperature range from 298 to 998 K.

From the density, we can estimate the diffusion speed of the hydrocarbon molecules in the argon buffer gas and the resulting random-walk-averaged diffusion length, i.e., the average distance the molecules diffuse during the residence time in the hot zone. This turns out to vary from ~9 to 12 mm over the experimental temperature range. The important point is that the diffusion length is ~10 times the tube radius, and thus the sample molecules diffuse back and forth across the tube bore many times during their passage through the hot zone. From the point of view of reaction kinetics, this has both good and bad consequences. The good news is that, even though our flow is laminar, all sample molecules spend approximately equal times in the fast and slow regions of the flow and thus have very similar residence times in the hot zone (i.e., pseudo plug flow). The average residence time is easily calculated from the mass-flow-weighted flow velocity.

Unfortunately, rapid diffusion means that we measure a combination of homogeneous and heterogeneous kinetics; thus, only phenomenological rate constants can be estimated. As noted below, wall collisions are clearly important in establishing the temperature distribution in the sample molecules; however, we see evidence for only minor contributions from walls reactions. Purely homogeneous kinetics could be measured with a much larger diameter flow tube, but the sample consumption rates would be too large to allow analysis of functionalized strained hydrocarbons, where only milligram samples are typically available.

The flow tube temperature, T_{nominal}, is measured by a thermocouple embedded just against the outside wall of the quartz capillary tube, in the center of the 10 cm long hot zone. Temperature is stable to 2 K. There are a number of important issues related to the temperature distribution and heat-up rate experienced by the molecules in the flow.

Particularly at high temperatures, the inner wall temperature might be significantly lower than the measured outer wall temperature, due to the power needed to bring the gas stream to temperature. From the flow rate and heat capacity (C_p(Ar) = 20.786 J/(mol·K)),[28] we estimate the gas heat-up power to be only ~8 mW at our maximum temperature (1000 K). The total power used to heat the flow tube to 1000 K is 88 W; thus, the gas heat-up power is negligible, and we are justified in assuming that the inner and outer wall temperatures are equal.

A more significant issue is the temperature profile along the length of the flow tube hot zone. To estimate the profile, the temperature was measured with thermocouples embedded against the outer wall at three positions along the length of the hot zone: at center and 5 mm from each end. Defining the center temperature as T_{nominal}, we find that the exit temperature equals T_{nominal} at low temperatures but is up to 6% low at the highest temperatures. The entrance temperature deviates more, by up to 15% at the highest temperatures. The larger deviation at the entrance reflects the fact that the flow tube is encased in a heavy copper jacket kept near room temperature up to a point ~3 cm from the entrance end of the hot zone. In contrast, the exit end is loosely coupled to the ion source inlet and thus has relatively little thermal load. Using a finite-difference heat transfer formulation given by White,[29] together with data from the three thermocouples, we estimated the flow tube temperature profile along the flow tube length. The important result is that the central 4−5 cm (i.e., half) of the hot zone is within 2% of T_{nominal}, even at our highest temperatures. At T_{nominal} of 500−700 K, where most of the chemistry occurs, this central, nearly isothermal region is about 60% of the hot zone length.

The final issue relating heat transfer is the how quickly the molecules in the flow stream reach the wall temperature. We operate in the laminar flow regime, with no turbulent mixing. Thus, the sample molecules heat up by two mechanisms: thermal conduction in the argon buffer gas and diffusion of the sample molecules to the flow tube wall. Given the diffusion behavior discussed above, each sample molecule undergoes ~10 wall collisions, or roughly one collision every centimeter along the hot zone. In each adsorption/desorption event, the molecules should equilibrate at the wall temperature. Including the additional heating by argon thermal conduction, it is clear that the internal temperature of the molecules along the flow tube length closely tracks the temperature profile of the walls.

For reference, the Damkohler number of our reactor, defined[30,31] as D_I = reactor residence time/reaction lifetime,

varies from 0 at room temperature to ~3.5 for norbornadiene at 973 K and from 0 to 4.5 at 873 K for quadricyclane. At $T > 873$ K the reaction lifetime for quadricyclane is too short to measure in our reactor. For toluene, cycloheptatriene, and cyclopentadiene, no reaction is observed ($D_I = 0$). As already noted, the diffusional mixing time and heat-up times are short compared to the residence time.

Materials. Quadricyclane (99%), norbornadiene (99%), toluene (99.5+%), cycloheptatriene (97%), and dicyclopentadiene (99%) were purchased from Aldrich and degassed by repeated freeze−pump−thaw cycles. Methane (99.99%), argon (99.998%), and xenon (99.995%) were purchased from Mountain Airgas and Spectra Gases, respectively, and used without further purification.

Data Analysis. Several types of experiments were performed. Ions are generated by methane chemical ionization (CI), and the basic experiment is measuring CI mass spectra as a function of flow tube temperature. The CI mass spectra are distinct for each of the precursor molecules, and this provides both a first-order fingerprint to identify the molecules and insight into the ionization dynamics. Variable flow tube temperature CI mass spectra (VT/CI) allow us to follow changes in molecules exiting the flow tube and thus determine thermal stability and decomposition pathways for the strained molecules. In the VT/CI mass spectra plotted below, each data set has been normalized to the total ion intensity in the mass range of *m*/*z* 50−200. This accounts for small changes in CI efficiency with temperature.

Positive identification of the isomeric structure of the molecules is obtained by low-energy collision-induced dissociation (CID), which can also be done as a function of temperature. This is done by selecting a particular ion from those generated by CI and then colliding the ion beam with xenon under single-collision conditions. As we demonstrated previously,[7] CID at sufficiently low collision energy is able to distinguish $C_7H_8^+$ derived from QC, NBD, and TOL. The CID patterns provide some clues as to the structures of the ions derived from the different isomer precursors and some insight into isomerization processes on the ionic potential surface. The changes in CID patterns with flow tube temperature reflect changes in the composition of neutral molecules exiting the flow tube. CID spectra are normalized to the intensity of the parent ion in question.

All experiments are repeated at least twice, and the relative uncertainties are approximately ±5%, largely due to the variation of pressure in the ion source. The data reported here are the average results.

III. Results and Discussion

A. Thermal Decomposition. *Toluene*. Variable temperature/chemical ionization (VT/CI) mass spectra of toluene are shown in Figure 3 for flow tube temperatures ranging from 298 to 973 K. The room-temperature mass spectrum has only one major peak at *m*/*z* 93, corresponding to the molecular weight plus one, $(M + 1)^+$. This ion is produced by proton transfer from hydrocarbon ions (principally CH_5^+) formed by ion−molecule chemistry in the methane CI reagent. As expected, there is a small peak at *m*/*z* 94 from natural abundance $^{13}C^{12}C_6H_9$. There is also a small, but analytically very important, peak at the molecular weight, *m*/*z* 92. This presumably results from charge-transfer ionization: $R^+ + C_7H_8 \rightarrow C_7H_8^+ + R$, where R^+ is some ion generated in the CI source. Electron impact (EI) ionization cannot be responsible for *m*/*z* 92 signal, because EI is found to give an extensive series of fragment ions.[7] The small peak at *m*/*z* 91 results from either H_2 elimination from the dominant $(M + 1)^+$ ion or hydride abstraction from neutral toluene by some ion present in the source.

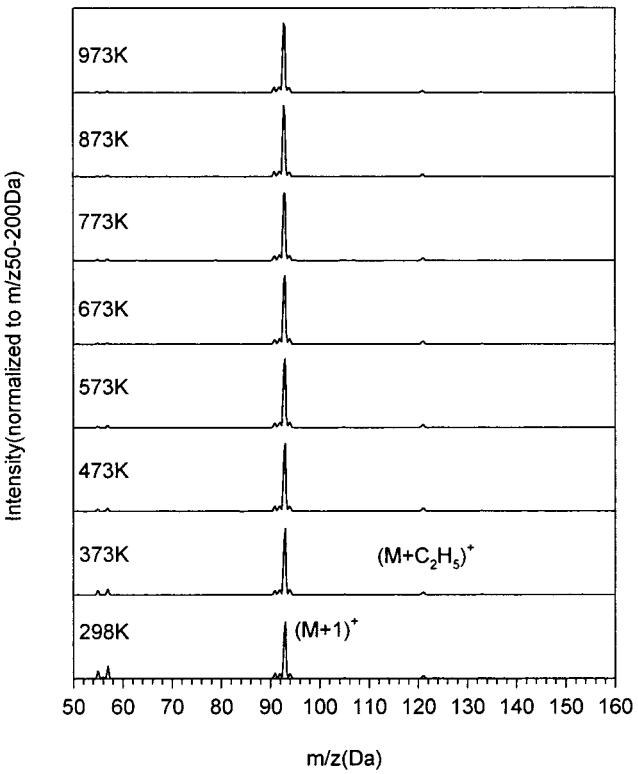

Figure 3. Variable flow tube temperature chemical ionization mass spectra of toluene.

Ion−molecule reactions of the methane CI reagent give rise to a hydrocarbon ion background spectrum with peaks at nearly every conceivable $C_xH_y^+$ mass. Fortunately, these background peaks only have significant intensity in the low mass portion of the spectrum. In order of decreasing intensity, the major background peaks are *m*/*z* 29 ($C_2H_5^+$), 17 (CH_5^+), 41 ($C_3H_5^+$), 19 (H_3O^+?), 27 ($C_2H_3^+$), and 43 ($C_3H_7^+$). In the high mass region plotted in the figures, the only significant background peaks are *m*/*z* 57 and 55 ($C_4H_9^+$ and $C_4H_7^+$). At the main masses of interest for detecting C_7H_8 isomers and their pyrolysis products, the hydrocarbon background is only a few percent of the signal level.

In addition to the main proton-transfer (PT) and charge-transfer (CT) ionization mechanisms, the hydrocarbon ions can form adducts with the analyte molecules, including the small peaks at *m*/*z* 105 $(M + CH)^+$, *m*/*z* 121 $(M + C_2H_5)^+$, and *m*/*z* 133 $(M + C_3H_5)^+$. As discussed below, these small adduct peaks are quite sensitive to parent neutral isomer energy and so form an important part of the mass spectral fingerprint.

As the flow tube temperature is raised to 973 K, no significant changes are observed in the CI mass spectrum, indicating that TOL is stable on our millisecond time scale. This suggests that if TOL is formed in decomposition of one of the strained precursors, the TOL product should be stable with respect to further decomposition. The fact that the TOL fingerprint does not change with flow tube temperature also supports our estimate that the ionization conditions are nearly independent of flow tube temperature.

Cycloheptatriene. VT/CI mass spectra were run for cycloheptatriene (CHT) as well, since this is one possible isomerization product. The spectra are similar to those discussed above for TOL. There is no evidence for thermal breakdown of CHT

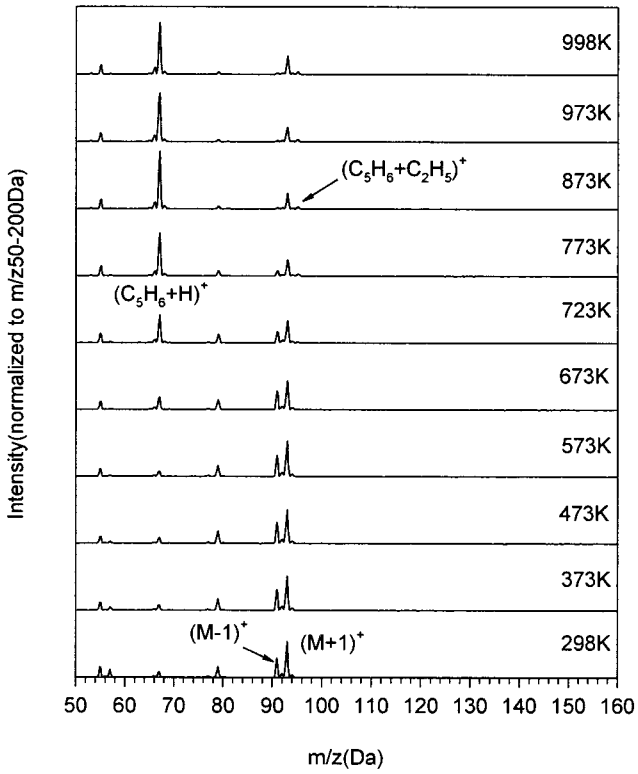

Figure 4. Variable flow tube temperature chemical ionization mass spectra of norbornadiene.

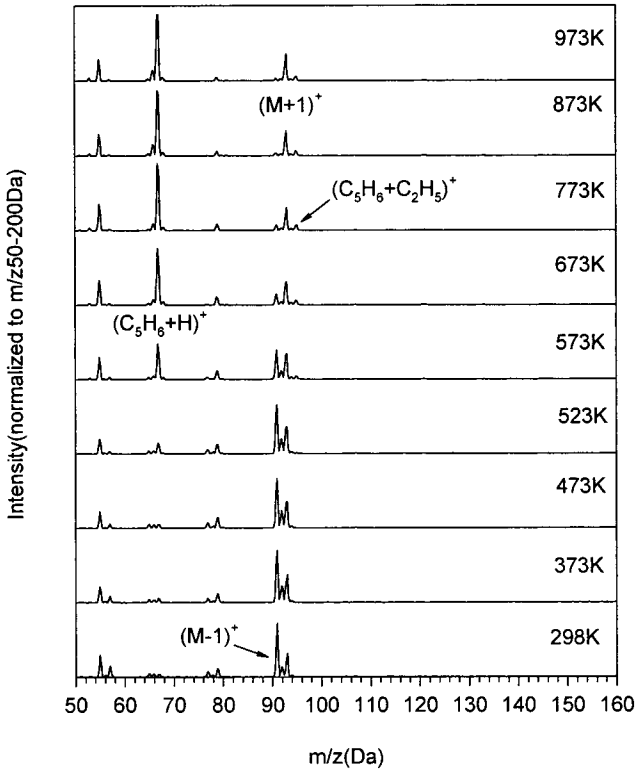

Figure 5. Variable flow tube temperature chemical ionization mass spectra of quadricyclane.

in our time/temperature range, and the spectrum is dominated by the $(M + 1)^+$ peak. It is difficult with CI mass spectra to distinguish TOL and CHT; however, there are some differences that allow us to at least estimate the high-temperature TOL/CHT branching in isomerization of the higher-energy isomers. The $(M + 1)^+/(M - 1)^+$ peak ratio is ~14 for TOL but ~11 for CHT. In addition, the $(M + C_2H_5)^+$ adduct peak is substantially smaller for TOL than for CHT. Our CI spectra for CHT and TOL are similar to those reported by Field.[32]

Norbornadiene. The VT/CI mass spectra of norbornadiene (NBD) are shown in Figure 4. The room-temperature spectrum again shows a prominent $(M + 1)^+$ (*m*/*z* 93) peak due to protonation of the neutral precursor, as well as the required ^{13}C-substituted analogue at *m*/*z* 94. There is also a substantial $(M - 1)^+$ peak at *m*/*z* 91, probably due to H_2 elimination from $(M + 1)^+$. The peak at *m*/*z* 67 is $C_5H_7^+$, which is attributed to C_2H_2 loss from the $(M + 1)^+$ parent ion. As with TOL, there are small peaks due to adducts at *m*/*z* 105 $(M + CH)^+$, *m*/*z* 121 $(M + C_2H_5)^+$, and *m*/*z* 133 $(M + C_3H_5)^+$. Unlike TOL, the *m*/*z* 121 peak is accompanied by peaks at 119 and 117, corresponding to loss of one or two H_2 molecules from the $(M + C_2H_5)^+$ adduct. Similarly, *m*/*z* 131 is seen to lose one or two H_2 units. The small peak at *m*/*z* 79 was attributed by Field[32] to loss of C_3H_6 from the $(M + C_2H_5)^+$ adduct. There is also barely visible peak at *m*/*z* 77 due to the CH_3 loss from M^+. A clear trend is that there is considerably more fragmentation of both $(M + 1)^+$ and the adducts, compared to the case of TOL. We attribute this to the higher ΔH_f of NBD being available to drive fragmentation in the resulting ions.

As with TOL, the low mass region of the NBD spectrum, including the *m*/*z* 55 and 57 peaks, is dominated by background hydrocarbon ions generated in ion−molecule reactions of methane in the source.

As the flow tube temperature is increased, no significant changes are observed in the range below 673 K, indicating that NBD is not decomposing during the flow tube residence time. Above this temperature the spectrum gradually changes with temperature up to 973 K and then no further change is observed at 998 K, the limit of our flow tube temperature. The following changes are observed: All peaks associated with the parent neutral decrease in intensity. The near-MW peaks, $(M - 1)^+$, M^+, and $(M + 1)^+$, all decrease, and the $(M - 1)^+/(M + 1)^+$ and $M^+/(M + 1)^+$ peak ratios also decrease such that only $(M + 1)^+$ is left with substantial intensity at high temperatures. The peaks at *m*/*z* 79, 117, 119, 129, and 131, attributed to H_2 or C_3H_6 loss from adducts, also decrease.

Some new peaks, attributed to pyrolysis products, appear over the same temperature range. The peak at *m*/*z* 67 ($C_5H_7^+$) and a new peak at *m*/*z* 95 gain intensity in concert. These peaks are both attributed to ionization of neutral C_5H_6, in one case by proton transfer and in the other by $(C_5H_6 + C_2H_5)^+$ adduct formation. C_5H_6 (cyclopentadiene) is expected to be a major decomposition product, since it can form by C_2H_2 elimination in a retro-Diels−Alder reaction. We do not detect a concomitant increase in ions that might result from the C_2H_2 product. The proton affinity of C_2H_2 is ~153.3 kcal/mol,[33] compared to ~199.6 kcal/mol for cyclopentadiene (C_5H_6), probably leading to lower detection efficiency. In addition, peaks in the hydrocarbon background spectrum at *m*/*z* 27 and 55 ($C_2H_3^+$ and $(C_2H_2 + C_2H_5^+)$) obscure any small changes in the most likely ions that would be generated from C_2H_2. There is a small increase in the *m*/*z* 55 ($C_4H_7^+$) peak; however, this could also be attributable to small changes in source conditions with flow tube temperature. In the high-temperature limit, the major peaks remaining are $(M + 1)^+$ at *m*/*z* 93 and the pair of peaks attributed to cyclopentadiene at *m*/*z* 67 and 95. The persistence of $(M + 1)^+$ indicates that some decomposition occurs via isomerization to a more stable C_7H_8 isomer.

Quadricyclane. The VT/CI mass spectra of QC are shown in Figure 5. At room temperature the spectrum is qualitatively

similar to that of NBD. The dominant peaks are $(M - 1)^+$, M^+, and $(M + 1)^+$, though the relative intensities of $(M - 1)^+$ and M^+ are higher with QC. The higher $(M - 1)^+$ intensity probably reflects the high ΔH_f of QC, which evidently is available to drive H_2 elimination from the nascent $(M + 1)^+$ ions produced by proton-transfer CI. The relatively strong M^+ signal, due to charge-transfer ionization, probably reflects reduced PT ionization due to the lower proton affinity of cycloalkanes compared to that of analogous unsaturated species.[33] As with NBD, a *m*/*z* 79 peak is observed, and by analogy we attribute this to C_3H_6 elimination from the $(M + C_2H_5)^+$ adduct ion. Little signal is observed for the $(M + C_2H_5)^+$ adduct itself, but a small peak is observed for *m*/*z* 117, corresponding to loss of two H_2 from the adduct. As with the $(M - 1)^+/(M + 1)^+$ ratio, we propose that the greater degree of adduct fragmentation, compared to the case of either NBD, TOL, or CHT, is attributable to release of the QC strain energy in the adduct ion.

For flow tube temperatures below 523 K, there are no appreciable changes in the spectrum, indicating that QC is stable on our time scale over this temperature range. At ~573 K, two distinctive changes are observed, indicating the onset of decomposition. Peaks appear at *m*/*z* 67 and *m*/*z* 95 corresponding to $(C_5H_6 + H)^+$ and $(C_5H_6 + C_2H_5)^+$, indicating that C_2H_2 elimination to give cyclopentadiene is occurring. Simultaneously, the intensity of the $(M - 1)^+$ and M^+ peaks decrease relative to $(M + 1)^+$, indicating that some decomposition via isomerization to a more stable C_7H_8 structure is occurring.

The QC pattern at 673 K is qualitatively similar to NBD at 773−873 K. The dominant decomposition pathway is C_2H_2 elimination resulting in C_5H_6, and there is a minor channel involving isomerization to a more stable C_7H_8 isomer.

B. VT Collision-Induced Dissociation: Isomer Identification and Dissociation Mechanisms. While it is straightforward to identify pyrolysis *fragments* by their masses, both NBD and QC also give a pyrolysis product at the molecular mass, i.e., an isomer. To identify these isomers and thus provide additional insight into the pyrolysis process, we performed variable temperature low-energy collision-induced dissociation (VT/CID) studies. As reported earlier,[7] we found that the $(M + 1)^+$ ions from all three isomeric precursors give CID spectra that are nearly identical; i.e., all information about molecular structure is lost in the proton-transfer process creating $(M + 1)^+$. As expected, CID of $(M - 1)^+$, probably created by H_2 elimination from $(M + 1)^+$, also is nearly independent of neutral precursor. This, together with the observation (see above) that both $(M + 1)^+$ and adduct ions suffer more fragmentation for QC and NBD, relative to TOL, suggests that the protonated or alkylated cations do not retain the neutral isomer structure.

Fortunately, we find that the M^+ ions, produced by CT, give CID spectra that are distinct for each neutral precursor, provided that the collision energy is sufficiently low. This indicates either that the cations retain the neutral structure or at least that they preserve some memory of the neutral structure. For example, one could imagine that ions derived from the higher-energy neutrals (QC and NBD) retain this extra energy and thus fragment differently in collisions. If this were the case, we would expect a higher fragmentation efficiency for ions derived from QC or NBD and perhaps a greater branching to higher-energy dissociation channels (Figure 1). In fact, as the results below show, the opposite is observed, leading us to conclude that CT ionization by methane is gentle enough that the majority of the M^+ ions retain the neutral structure.

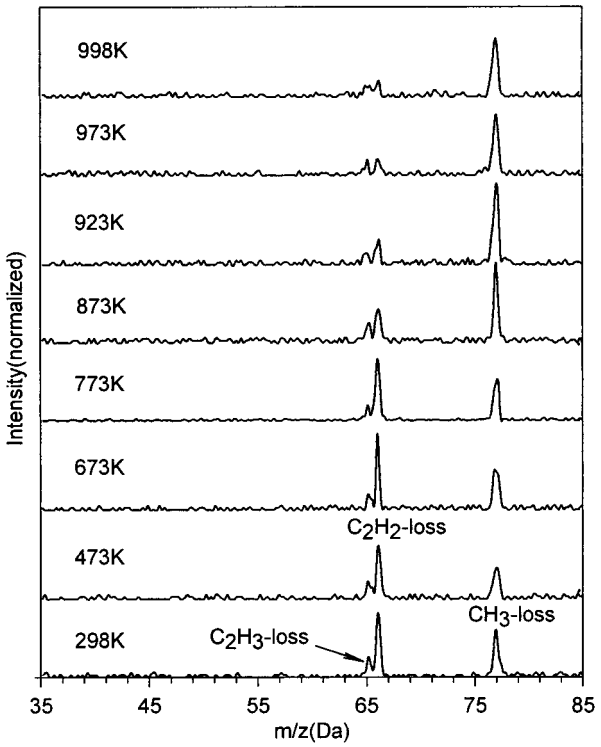

Figure 6. Variable flow tube temperature chemical ionization/low-energy CID spectra of NBD.

Toluene. For TOL, the low-energy (~3 eV center of mass) CID behavior shows no significant changes with temperature, as expected from the invariant VT/CI spectra given in Figure 3. This confirms that TOL does not decompose under our conditions. The only significant product is *m*/*z* 77, $C_6H_5^+$, corresponding to methyl loss. It is possible that there might be a small branching to H loss as well, but this is difficult for us to determine because the low collision energy and single-collision conditions required to identify QC and NBD result in low dissociation yields, and any small signal for $(M - 1)^+$ would be buried under the low mass tail of the primary ion signal. As Figure 1 shows, C_2H_2 elimination is considerably lower in energy than methyl loss, and as shown below, C_2H_2 elimination dominates the CID products for NBD and QC. Its absence for TOL suggests that the collisionally activated cation does not sample configurations with NBD or QC structures.

Norbornadiene. Figure 6 gives CID spectra ($E_{collision} = 2.9$ eV) for NBD as a function of temperature, where each spectrum is normalized to the intensity of the M^+ parent peak (*m*/*z* 92, off scale). The strongly temperature-dependent fragmentation behavior provides structural evidence for the isomeric pyrolysis product. The room-temperature CID spectrum shows three significant fragmentation channels characteristic of M^+ derived from the NBD isomer: CH_3 loss (*m*/*z* 77), C_2H_2 loss (*m*/*z* 66), and C_2H_3 loss (*m*/*z* 65). (Note: ~4% of the *m*/*z* 65 peak is due to C_2H_2 loss from ^{13}C $(M - 1)^+$ ions.) For NBD, the dominance of the energetically favored C_2H_2 elimination channel is not surprising, because this elimination can occur via a retro-Diels−Alder reaction from the NBD^+ structure. The observation of a substantial component of CH_3 elimination suggests that, in some cases, collisional activation is able to drive isomerization to TOL prior to fragmentation.

For flow tube temperatures below 700 K, the VT/CI results in Figure 4 show no NBD decomposition, and as expected, the CID spectra are also invariant over this temperature range. At 773 K and higher, the VT/CI results show increasing decom-

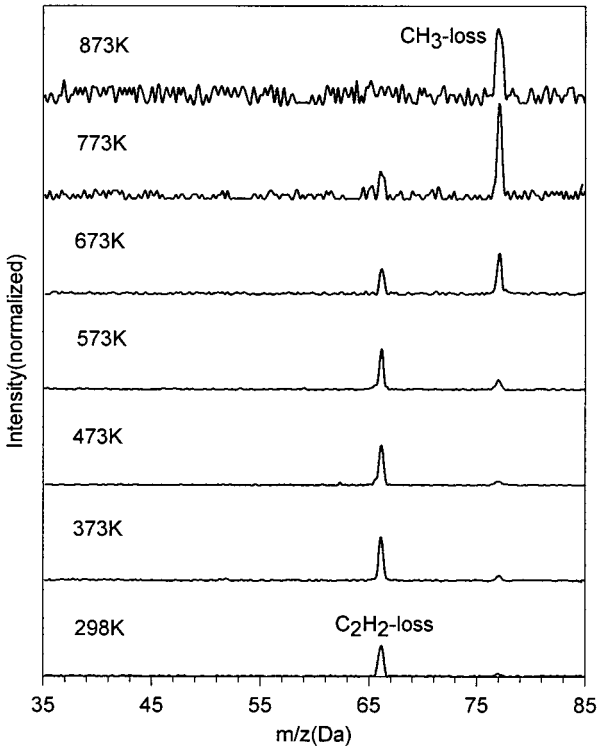

Figure 7. Variable flow tube temperature chemical ionization/low-energy CID spectra of QC.

position, which is essentially complete by 973 K. Over this same flow tube temperature range the M^+ CID spectra also change such that, by high temperatures, only methyl loss fragmentation is observed. This high-temperature CID pattern is identical to that for TOL, suggesting that TOL is likely to be the pyrolysis product. As discussed below, it is possible that cycloheptatriene (CHT) accounts for some of the isomerization product as well, but at high temperatures the isomer product appears to be mainly TOL.

Quadricyclane. The CID spectra for $M^{\cdot +}$ parent ions derived from QC are shown in Figure 7, for a collision energy of 2.9 eV. At temperatures under 500 K, where the QC is not decomposed in the flow tube, the major CID peak corresponds to C_2H_2 loss, and there is a small peak corresponding to CH_3 loss as well. Note that the 2.9 eV collision energy is substantially higher than the activation barrier for $QC^+ \rightarrow NBD^+$ isomerization. The fact that the fragmentation pattern is substantially different for QC and NBD-derived M^+ suggests that the QC-derived M^+ is not isomerized in the source and that the collision-induced fragmentation pathway does not involve a hot NBD^+ intermediate. One possibility is that the collisionally activated QC^+ fragments in the course of the isomerization, due to the sudden release of the strain energy.

As an interesting aside, we note that the relative contribution of the methyl loss channel increases dramatically with increasing collision energy. By $E_{\text{collision}} \sim 6$ eV, the CH_3 and C_2H_2 loss peaks are equal, and at higher energies methyl loss dominates. This suggests that if we could do the experiment in the limit of zero excess energy (and zero signal), only C_2H_2 loss would be observed. As Figure 1 shows, methyl loss is a higher-energy channel than C_2H_2 loss. It is not obvious which channel might have the lower activation barrier, however, since we are starting from $C_7H_8^+$ with the QC structure, and either reaction requires rearrangement. The dominance of C_2H_2 elimination at low collision energies indicates that this has the lowest activation energy of the two channels. The observation that CH_3 loss rapidly becomes dominant indicates that the transition state for this channel must be substantially looser, as might be expected if the CC bond rupture is the rate-limiting step.

At 573 K flow tube temperature, the CID spectrum begins to change, with an increase in the relative contribution of methyl loss. The signal/noise ratio in the high-temperature spectra is substantially degraded simply because the intensity of M^+ parent ions in the high-temperature CI spectra is greatly reduced. The trend toward increasing CH_3 loss continues with increasing temperature, such that by 873 K only the CH_3 loss peak remains. As for NBD, the CID spectrum and CI peak ratios at high temperatures are consistent with the isomerization product being TOL, though there appears to be some CHT production at low temperatures (see below).

C. Pyrolysis Kinetics and Branching. *Data Fitting*. The CI mass spectrum measured at any given flow tube temperature is a linear combination of mass spectra for the individual molecular components present in the flow tube eluent. For example, we expect that the NBD spectra over our temperature range may have contributions from ionization of NBD, C_5H_6, C_2H_2, TOL, and CHT, and perhaps other molecules. To estimate quantitative pyrolysis behavior from the experimental data, we need to analyze the variable temperature CI spectra, extracting the temperature dependence for each molecular component. A fundamental assumption in this analysis is that the mass spectral pattern (i.e., ratios of peak intensities) of a particular component molecule is, other than total intensity, independent of flow tube temperature. The experimental justification for this is that the ion source conditions (partial and total pressure and temperature) are nearly independent of flow tube temperature, and thus the mass spectral pattern of any given molecule should also be nearly constant. Evidence supporting this argument is given by the unchanging TOL CI spectra given in Figure 3 and the nearly constant pattern of hydrocarbon background ions. The goodness of the fits below further justify this assumption.

Two approaches were taken to fitting the data. For TOL and NBD, where the number of components (product species) is relatively small, we first tried factor analysis.[34,35] In essence, this consists of extracting a set of orthogonal eigenvectors that are capable of describing the changes in CI spectra as a function of temperature. These eigenvectors must then be projected (rotated) to generate chemically reasonable (i.e., nonnegative) mass spectra of the molecular components making up the CI spectrum. The advantage of the factor analysis approach is that no assumptions need be made regarding the number or nature of the components making up the spectra. The problem is that rotating the eigenvectors into a chemically reasonable set of molecular mass spectra becomes difficult for high-dimensional problems such as the QC pyrolysis, where there is reason to anticipate the presence of five independent components contributing over the experimental temperature range.

This prompted use of a simple iterative least-squares fitting approach. The fitting program is based on the three assumption: (1) The CI mass spectrum of each molecular component is independent of temperature. (2) The total mass spectrum at each temperature is a linear combination of component spectra. (3) The coefficient of each component is nonnegative, and the coefficients sum to unity. As in factor analysis, we attempt to fit the spectra at each temperature to a linear combination of basis spectra (i.e., spectra for individual molecular components). In the iterative fitting approach, however, the basis spectra are generated using our qualitative understanding of the CI spectra, and the fitting reduces to simply finding the contribution of each

basis spectrum to the total spectrum at each temperature. By starting with chemically reasonable basis spectra, we avoid the rotation problem of the factor analysis approach. The disadvantage is, of course, that the fits require a qualitative understanding of the pyrolysis behavior so that we can intelligently chose basis spectra. For NBD and TOL, where we were able to use both factor analysis and the iterative approach, the resulting component spectra and fitting coefficients are essentially identical. This is not surprising, but it confirms the qualitative understanding used to generate the component spectra. The quality of the iterative fits is excellent. The average root-mean-square deviation is in the range between 0.1 and 1.5%. For each molecule we have at least three different VT/CI data sets to fit. The temperature dependence of the various fit components is reproducible, but there are small changes in the branching between fit components from run to run. These deviations result from the signal/noise of the spectra and from small run-to-run changes in the hydrocarbon background peaks in the spectra. From the deviations for different data sets, we estimate that the random fitting error is about 5% for any given component.

The basis spectra are simply mass spectra for each starting material and for species generated in each pyrolysis product channel. For TOL, CHT, NBD, and QC parent molecule components we simply used the CI spectra for each pure material. On the basis of the discussion above, it is clear that in pyrolysis of NBD the two major channels are fragmentation to $C_5H_6 + C_2H_2$ and isomerization to TOL and/or CHT.

The fits shown below give the contributions extracted for both TOL and CHT isomeric products. As noted above, however, the CI basis spectra for TOL and CHT differ only in the intensities of two minor peaks, and this results in uncertainty in determining the TOL/CHT branching. We feel that the total contribution of TOL + CHT is well determined (5% uncertainty), and the trends in TOL/CHT branching with temperature are correct but are not able to give a firm uncertainty estimate for the TOL/CHT branching.

To generate the $C_5H_6 + C_2H_2$ basis spectrum, we simply took the high-temperature NBD spectrum and subtracted out the TOL/CHT contribution. This gives a "spectrum of everything left",but the only significant peaks in the $m/z > 50$ mass range are due to C_5H_6. To verify that this residual spectrum is consistent with cyclopentadiene, we ran a series of CI mass spectra for pure cyclopentadiene over the temperature range from 473 to 973 K and find that it matches the residual spectrum closely. This confirms production of c-C_5H_6 as the major NBD and QC pyrolysis product and also demonstrates that c-C_5H_6 itself is stable over our temperature range. Cyclopentadiene for these experiments was generated from the dimer by warming to 90 °C, and this warming is why our lowest temperature c-C_5H_6 spectrum is at 473 K.

For quadricyclane, we included basis spectra for TOL, CHT, NBD, $C_5H_6 + C_2H_2$, and the QC parent molecule. From the observation that these five components give excellent fits to the entire QC data set, we conclude that there are no other significant species present over our temperature range.

Note that the fitting gives the fraction of the total ion signal ($50 < m/z < 200$) arising from each neutral compound. What we would like to know is the fractional composition of each compound in the neutral gas exiting the flow tube. Unfortunately, this requires knowing the total ionization efficiency for each compound under the conditions of our experiment, and we do not have this information. Most ionization is by proton transfer, and the relative PT efficiency might be expected to depend on the exoergicity of the $RH^+ + M \rightarrow (M + 1)^+ + R$ reaction, where RH^+ is one of the ions produced by ion chemistry in the methane CI reagent (e.g., CH_5^+ or $C_2H_5^+$). For both TOL and c-C_5H_6 the proton affinities (189.8 and 199.6 kcal/mol, respectively[33]) are large compared to those of CH_4 and C_2H_4 (132 and 162.6 kcal/mol); thus, it seems reasonable to estimate that they should have similar PT ionization efficiencies. For both TOL and C_5H_6 there is also substantial ionization by $M-C_2H_5^+$ adduct formation, and since both molecules are unsaturated cyclic species, it seems reasonable to assume that adduct formation efficiency might be roughly equal. Within these assumptions, the pyrolysis branching ratios should be similar to the ion branching plotted in the figures.

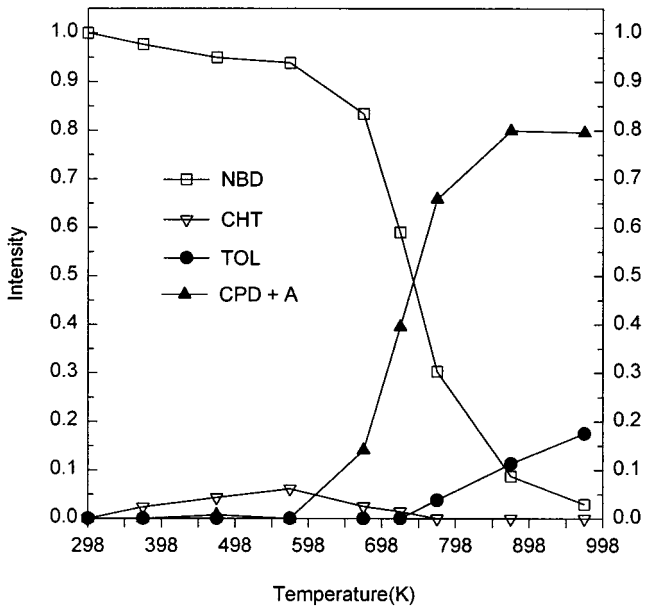

Figure 8. Composition of flow tube output as a function of temperature for NBD.

Toluene. As expected from the CI spectra themselves, there is no significant change in fit composition for TOL over our temperature range. In the iterative fitting approach this is reflected by only the TOL component spectrum having a significant contribution to any of the temperature-dependent spectra. The factor analysis results concur —a single factor can account for over 99.7% of the total variance in the series of spectra.

Norbornadiene. The NBD fitting results, shown in Figure 8, show a small decrease in NBD signal, with a concomitant increase in CHT signal for temperatures up to ~700 K. Above ~700 K the NBD signal rapidly decreases, and the C_2H_2 elimination channel (C_5H_6) dominates the product distribution. At temperatures above 800 K, signal due to TOL grows in, while the C_5H_6 signal decreases slowly, suggesting that at higher temperatures TOL might become the dominant channel.

Halper et al. reported[13] that NBD decomposes by C_2H_2 elimination (to C_5H_6) and by isomerization to cycloheptatriene (CHT) with roughly equal rates. TOL was reported as only a minor product. In their experiment, NBD was subjected to temperatures of 673−748 K in steel or stainless steel vapor-phase reactors at atmospheric pressure and 1−28 s residence times. The mechanism for this pyrolysis was then examined by Woods.[12] In Woods' experiments, the ratio of TOL/CHT increased substantially with residence time at ~748 K. This result suggested that CHT was formed initially and subsequently rearranged to TOL. In our experiments we tentatively conclude that the major *high-temperature* isomerization product is TOL.

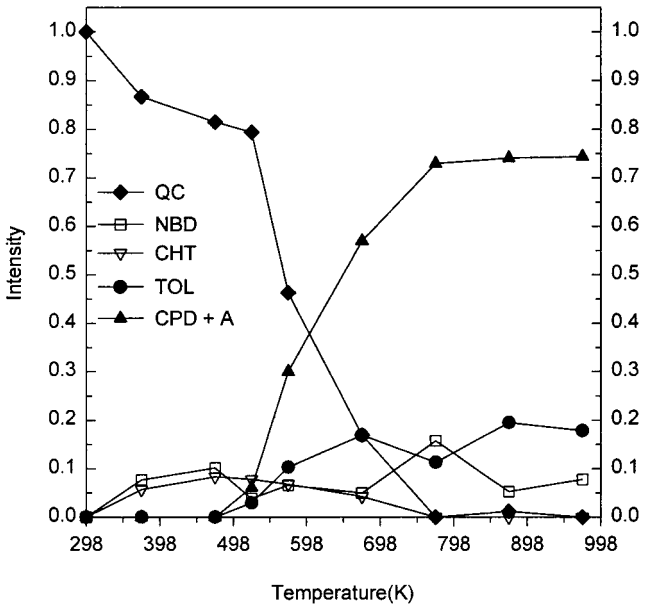

Figure 9. Composition of flow tube output as a function of temperature for QC.

Given Woods' observation, it seems reasonable that our higher temperatures would generate more TOL.

Birely and Chesick[10] report activation energies for NBD decomposition as follows: NBD → C_5H_6 + C_2H_2, 211 kJ/mol; NBD → CHT, 216 kJ/mol. (Note: Lishan et al.[11] quoted energetics from Birely and Chesick; however, they interchanged the activation energies for the two reactions.) Our data are consistent with the earlier kinetic results in this regard. The higher-temperature onset for isomerization relative to the acetylene elimination channel indicates that the isomerization channel has the higher activation energy. In addition, the observation that the relative branching to isomerization increases with temperature suggests that isomerization involves a looser transition state than the C_2H_2 elimination reaction. This conclusion is consistent with the higher preexponential factor reported by Birely and Chesick for the isomerization reaction.

One curious feature of our results is the small amount of apparent conversion from NBD to CHT at temperatures below 600 K. The growth in apparent CHT signal is just outside our estimated 5% fitting uncertainty; however, it is consistent across all data sets. As Figure 4 shows, there are no significant changes in the CI spectra over this temperature range, and we conclude that apparently the low-temperature CHT production is an artifact and that the true unimolecular decomposition sets in above 600 K. This conclusion is also consistent with other observations. As noted, the lowest-energy decomposition pathway for NBD is C_2H_2 elimination; thus, the low-temperature reaction should not be dominated by CHT production. In addition, the apparent CHT fraction is very weakly temperature-dependent, unlike behavior expected for an activated decomposition process.

It is not clear what causes this low-temperature background. One possibility is a wall-catalyzed isomerization, although we note that Birely and Chesick[10] reported that glass surfaces did not catalyze NBD decomposition significantly at similar temperatures. More likely, there are simply small changes in ion source conditions with flow tube temperature, unrelated to any actual kinetics, and the analysis program is best able to fit the changes by adding some CHT branching.

Quadricyclane. For quadricyclane the pyrolysis behavior, shown in Figure 9, is similar to that observed for NBD, the principal difference being that the pyrolysis begins at much lower temperatures. As with NBD, there is a small and weakly temperature-dependent change in the fitting results below ~500 K, and we again conclude that these changes are an artifact of changes in ionization conditions or possibly wall reactions.

From the raw data (Figure 5) it is clear that real spectral changes are present in the 523 K spectrum, and decomposition rapidly goes to completion at higher temperatures. At 523 K, QC-derived ions account for ~85% of the total, while at 673 K, the QC-derived fraction is only ~20%, and there is no QC-derived signal at higher temperatures. At our highest temperatures, the branching is dominated by acetylene elimination to give cyclopentadiene, with isomerization to TOL/CHT/NBD accounting for the balance of the signal. C_2H_2 elimination and isomerization turn on at approximately the same temperature, unlike the case of NBD, where isomerization is seen only at high temperatures.

Pyrolysis of QC was first reported by Dauben and Cargill more than three decades ago.[16] In this study, the pyrolysis was performed by sealing QC under nitrogen atmosphere in a Pyrex tube that was heated at 473−493 K for 5 min. The only product obtained was NBD, identified by infrared spectra and gas chromatography (GC). Hammond et al. also reported that QC isomerizes to NBD while being heated to 413−473 K.[17] Lishan et al.[11] reported a photolysis study of QC where the sample was excited to various CH stretching overtones. Products were quantified by GC. They observed a few percent dissociation to cyclopentadiene + acetylene, with the bulk of the products being NBD, TOL, and CHT.

Our results are significantly different from the literature thermal pyrolysis experiments, but this is not surprising in light of the different experimental conditions. Because our experiments are sensitive to faster rates, we see pyrolysis at temperatures 200−300 K higher than in the previous studies. In addition, we operate at several orders of magnitude lower pressure (both total and QC partial pressure); thus, the frequency of stabilizing collisions is lower in our experiments. Finally, we detect products directly after exiting the flow tube reactor, while previous experiments have used off-line GC analysis. In the previous low-temperature pyrolysis experiments, the population of molecules excited enough to undergo QC → NBD isomerization is small. After the activated molecules cross the barrier (Figure 1) between QC and NBD, they undergo rapid thermalizing collisions. Because the barriers for further decomposition of NBD are high, the thermalized NBD is expected to be stable under low-temperature conditions. In our experiments, the temperatures are higher and the frequency of stabilizing collision is lower, so that nascent NBD product molecules have a high probability for further isomerization or dissociation to final products. Our high-temperature pyrolysis results are more similar to the overtone photolysis experiments of Lishan et al.[11] Because the overtone excitation produces highly excited QC molecules, they also see conversion to C_5H_6 + C_2H_2, TOL, and CHT, as well as NBD.

From Figure 1 and from the literature it seems likely that the reaction path from QC to final products should pass through the NBD configuration, and in that case we might expect that the QC pyrolysis results should be rather similar to those of NBD. That is correct, with one exception. For NBD pyrolysis, the C_5H_6 + C_2H_2 product channel turns on at substantially lower temperatures than the isomerization to TOL. For QC pyrolysis, the same two channels are observed, but both turn on at approximately the same temperature. Consideration of Figure 1 suggests an explanation. QC molecules with enough excita-

TABLE 1: Effective Decomposition Lifetimes for QC and NBD

temp (K)	τ_{NBD} (ms)	τ_{QC} (ms)	temp (K)	τ_{NBD} (ms)	τ_{QC} (ms)
373	>40	>40	773	~1.9	<0.5
473	>40	~25.9	873	~0.6	<0.5
573	>40	~4.2	973	<0.5	<0.5
673	~11.9	~1.5	998	<0.5	<0.5

tion energy to pass over the ~141 kJ/mol activation barrier[9] for isomerization to NBD will produce NBD molecules with at least 230 kJ/mol internal excitation, i.e., ~10−20 kJ/mol in excess of the barriers for NBD → TOL/CHT or NBD → C_5H_6 + C_2H_2. Both isomerization and C_2H_2 elimination channels are, therefore, expected to be observed following the rate-limiting initial QC → NBD step.

Surface vs Homogeneous Chemistry. One question regarding interpretation of our results is the degree to which reactions catalyzed by the quartz wall of our flow tube contribute to the products. As discussed above, it is clear that wall collisions are important in bringing the sample molecules up to the flow tube temperature, but our results show no clear evidence for wall-catalyzed reactions. In the case of NBD, Birely and Chesick[10] attempted to determine the influence of surface chemistry by comparing experiments with their reactor empty and packed with glass beads. No effect was observed, and they concluded that glass surfaces are ineffective in catalyzing NBD decomposition in their temperature range (600−650 K).

We have examined our flow tube surface following a long series of runs with NBD and QC, and see no evidence for deposition of carbonaceous material; thus, we can rule out reactions that deposit material. The only direct evidence that *might* suggest some wall-catalyzed chemistry is the apparent, low-temperature isomerization behavior that shows up in the fits. As noted above, we suspect that this "chemistry" may be just an artifact of fitting small changes in the ion source conditions; however, wall chemistry is a possibility. Our tentative conclusion is that the chemistry we are observing is mostly homogeneous.

We note, however, that in a previous experimental series using a different flow tube we did see evidence for probable surface reactions. For that flow tube, the results for TOL and NBD were virtually identical to those reported here, and this was also true for QC at low temperatures. At high temperatures, however, QC was found to undergo polymerization/fragmentation reactions that are not observed in the reported data. The two flow tubes were nominally identical, and the reason for the difference in chemistry is unknown, although we suspect possible metal contamination of the inner quartz wall of the first tube. The absence of the previously observed wall reactions in the current data reinforces our belief that we are observing primarily gas-phase reactions.

Kinetics. To help separate the true temperature dependence of the decomposition kinetics from the temperature-dependent residence time in the flow tube hot zone, we have calculated effective decomposition lifetimes: $\tau = -t_{res}/\ln(I/I_0)$, where t_{res} is the mass-flow-weighted average residence time. For this calculation we have use the effective length of the hot zone of the tube, i.e., the length where the temperature is within 2% of $T_{nominal}$ (see above). In the temperature range of greatest interest, the effective length is between 100% and 60% of the heated zone length. The results, given in Table 1, are *effective* lifetimes; i.e., they assume first-order kinetics and include decomposition due to all processes including homogeneous and heterogeneous reactions.

Because our flow tube hot zone is not variable length (movable or multiple inlets are precluded by the requirement for a small bore), we are only able to determine lifetimes in the range from ~40 to ~0.5 ms. This, however, is the important time scale for many combustion applications. We have not attempted to estimate evolution rates for individual products due to the complication, noted above, of unknown relative ionization efficiencies. Nonetheless, we believe that ionization efficiencies are probably similar for the reactant and product species; thus, approximate evolution rates can be determined from the product branching.

IV. Conclusions

The VT/FTR/CI/MS and VT/FTR/CI/CID method has been tested on the pyrolysis of QC/NBD/TOL/CHT isomers. TOL and CHT are stable over the temperature range up to1000 K for millisecond residence times. NBD decomposes to cyclopentadiene plus acetylene and isomerizes to toluene and possibly cycloheptatriene at temperatures above ~700 K. The decomposition of QC is qualitatively similar to that of NBD. QC decomposes to cyclopentadiene plus acetylene and isomerizes to toluene at temperatures above 523 K. Under high-temperature/low-pressure conditions, stabilization of NBD produced in QC decomposition is inefficient.

Acknowledgment. We thank Prof. Joel M. Harris and Mr. James A. Kleimeyer for their help with the factor analysis. This work is supported by the Office of Naval Research, Mechanics and Energy Conversion Division (Dr. Gabriel Roy), under Grant N00014931073.

References and Notes

(1) Marchand, A. P.; Liu, Z.; Rajagopal, D.; Sorokin, V. D.; Zaragoza, F.; Zope, A. New High Energy/High Density Fuel Systems: Synthesis and Characterization. In *Proceedings of the 7th ONR Propulsion Meeting*; State University of New York at Buffalo: Buffalo, NY, 1994; pp 82−90.

(2) Marchand, A. P. *Chem. Rev.* **1989**, *89*, 1011−33.

(3) Eaton, P. E. An Introduction to Cubane and its Chemistry. In *Proceedings of the 7th ONR Propulsion Meeting*; State University of New York at Buffalo: Buffalo, NY, 1994; pp 117−129.

(4) Schmitt, R. J.; Bottaro, J. C.; Eaton, P. E. *Proc. SPIE−Int. Soc. Opt. Eng.* **1988**, *872*, 30−7.

(5) Griffin, G. W.; Marchand, A. P. *Chem. Rev.* **1989**, *89*, 997−1010.

(6) Moriarty, R. M.; Rao, M. Energetic Azide Compounds. In *Proceedings of the 7th ONR Propulsion Meeting*; State University of New York at Buffalo: Buffalo, NY, 1994; pp 75−81.

(7) Li, Z.; Eckwert, J.; Lapicki, A.; Anderson, S. L. *Int. J. Mass Spectrom. Ion Processes* **1997**, *167/168*, 269−79.

(8) Lias, S. G.; Bartmess, J. E.; Liebman, J. F.; Holmes, J. L.; Levin, R. D. *J. Phys. Chem. Ref. Data* **1988**, *17* (Suppl. 1).

(9) Bach, R. D.; Schilke, I. L.; Schlegel, H. B. *J. Org. Chem.* **1996**, *61*, 4845−47.

(10) Birely, J. H.; Chesick, J. P. *J. Phys. Chem.* **1962**, *66*, 568−570.

(11) Lishan, D. G.; Reddy, K. V.; Hammond, G. S.; Leonard, J. E. *J. Phys. Chem.* **1988**, *92*, 656−660.

(12) Woods, W. G. *J. Org. Chem.* **1958**, *23*, 110−112.

(13) Halper, W. M.; Gaerther, G. W.; Swift, E. W.; Pollard, G. E. *Ind. Eng. Chem.* **1958**, *50*, 1131−1134.

(14) Dauben, W. G.; Cargill, R. L. *Tetrahedron* **1961**, *12*, 186−189.

(15) Roquitte, B. C. *Can. J. Chem.* **1964**, *42*, 2134−2137.

(16) Dauben, W. G.; Cargill, R. L. *Tetrahedron* **1961**, *15*, 197−201.

(17) Hammond, G. S.; Turro, N. J.; Fischer, A. *J. Am. Chem. Soc.* **1961**, *83*, 4674−4675.

(18) Gunion, R. F.; Karney, W.; Wenthold, P. G.; Borden, W. T.; Lineberger, W. C. *J. Am. Chem. Soc.* **1996**, *118*, 5074−5082.

(19) Lee, H. S.; DePuy, C. H.; Bierbaum, V. *J. Am. Chem. Soc.* **1996**, *118*, 5068−73.

(20) Kuck, D. *Mass Spectrom. Rev.* **1990**, *9*, 187−233.

(21) Philippopoulos, C.; Economou, D.; Economou, C.; Marangozis, J. *Ind. Eng. Chem. Prod. Res. Dev.* **1983**, *22*, 627−633.
(22) Philippopoulos, C.; Marangozis, J. *Ind. Eng. Chem. Prod. Res. Dev.* **1984**, *23*, 458−466.
(23) Canas, L. R.; Greenberg, D. B. *Sol. Energy* **1985**, *34*, 93−99.
(24) Lahiry, S.; Haldar, C. *Sol. Energy* **1986**, *37*, 71−73.
(25) Smolanoff, J.; Lapicki, A.; Anderson, S. L. *Rev. Sci. Instrum.* **1995**, *66*, 3706−8.
(26) Daly, N. R. *Rev. Sci. Instrum.* **1960**, *31*, 264.
(27) Geankoplis, C. J. *Transport Processes and Unit Operations*, 3rd ed.; PTR Prentice Hall: Englewood Cliffs, NJ, 1993.
(28) Chase, M. W., Jr.; Davies, C. A.; Downey, J. R., Jr.; Frurip, D. J.; McDonald, R. A. *J. Phys. Chem. Ref. Data* **1985**, *14* (Suppl. 1).
(29) White, F. M. *Heat Transfer*; Addison-Wesley Publishing: Reading, MA, 1984.
(30) Penner, S. S. Similarity analysis for chemical reactions and the scaling of liquid fuel rocket engines. Presented at the 6th and 7th AGARD combustion panel meetings, 1954, Scheveningen, The Netherlands, Pairs, France.
(31) Williams, F. A. *Combustion Theory*, 2nd ed.; Benjamin/Cummings Publishing: Princeton, NJ, 1985.
(32) Field, F. H. *J. Am. Chem. Soc.* **1967**, *89*, 5328−5334.
(33) Lias, S. G.; Liebman, J. F.; Levin, R. D. *J. Phys. Chem. Ref. Data* **1984**, *13*, 695−808.
(34) Malinowski, E. R. *Factor Analysis in Chemistry*, 2nd ed.; Wiley: New York, 1991.
(35) Fister, J. C., III.; Harris, J. M. Factor analysis of transient Raman scattering data to resolve spectra of ground- and excited-state species. In *Computer Assisted Analytical Spectroscopy*, 1st ed.; Brown, S. D., Ed.; Wiley: New York, 1996.